*Ab initio* lattice dynamics of MnO



2009 J. Phys.: Condens. Matter 21 275402

(http://iopscience.iop.org/0953-8984/21/27/275402)

J. Phys.: Condens. Matter **21** (2009) 275402 (6pp) doi:10.1088/0953-8984/21/27/275402

# *Ab initio* lattice dynamics of MnO

**Urszula D Wdowik**[1] **and Dominik Legut**[2,3]

[1] Institute of Technology, Pedagogical University, PL-30-084 Cracow, Poland
[2] Institute of Physics of Materials, Academy of Sciences of the Czech Republic, CZ-616 62 Brno, Zizkova 22, Czech Republic
[3] Department of Physics, Uppsala University, PO Box 530, SE-751 21 Uppsala, Sweden

E-mail: legut@ipm.cz

Received 14 January 2009, in final form 4 May 2009
Published 10 June 2009
Online at stacks.iop.org/JPhysCM/21/275402

**Abstract**

Vibrational dynamics of the MnO lattice has been studied using density functional theory combined with the direct method. Considerations have been limited to the harmonic approximation. *Ab initio* calculated Hellmann–Feynman forces were used to obtain density of states and the dispersion relations of phonons in the MnO crystal. Corrections for the local Coulomb interactions were applied. The Hubbard energies were varied from 1 to 7.9 eV. Increased Hubbard terms give a significant increase in the on-site force constants of cations, while the force constants on anions are affected indirectly. The density of phonon states and the dispersion curves are shifted to higher frequencies with the increasing Hubbard energies. The on-site Coulomb interactions influence mainly the optical phonon vibrations. The higher Hubbard terms lower the mean-squared vibrations of both cations and anions. The lattice contribution to the heat capacity experiences small changes upon variation of Coulomb repulsion. Results of the calculations are compared to the existing experimental data.

## 1. Introduction

The simple 3d transition-metal oxides (MnO, FeO, CoO, NiO) form an important class of materials due to their several electrical and magnetic properties of practical utility. They are also important from a theoretical point of view since they serve as benchmark materials for the study of correlated electron systems [1, 2]. These oxides still challenge the theory of strongly correlated electron systems since they reveal difficulties in finding suitable models to explain their properties [3]. The highly correlated nature of electron interactions govern both the electronic structure and the lattice dynamics of 3d transition-metal oxides [4–6]. Therefore, the study of the vibrational dynamics of these oxides has become a subject of experimental [8–13] and theoretical investigations [4–7, 14–18].

Manganese oxide, MnO, is an example of an antiferromagnetic system with a type-II ordering (AFII). In the AFII ordering the magnetic moments of transition-metal cations are parallel within the (111) planes and they are antiparallel between the adjacent (111) planes. Hence, the spin-up and spin-down cations form two ferromagnetic sublattices and the AFII supercell is twice as large as the crystallographic unit cell. In the paramagnetic phase, MnO has a rocksalt structure (space group $Fm\bar{3}m$) with a lattice constant of 4.445 Å [19]. Below the Néel temperature of 118 K [20, 21], a small rhombohedral distortion along the ⟨111⟩ direction accompanies the transition to the AFII state. The distorted structure has a space group $R\bar{3}m$. The magnetic cell parameter equals 8.873–8.863 Å, while a deviation from cubic symmetry amounts to 0.3°–0.6° [22, 23]. Due to such small distortion the dynamic properties of the MnO lattice are frequently investigated under the assumption of perfect cubic symmetry [5].

Nowadays, computational methods based on density functional theory (DFT) employ the corrections for strong on-site Coulomb interactions between 3d electrons [1–3]. Interactions between correlated states are usually described by the Hubbard potential $U$ and the local exchange interactions are taken into account via the term $J$ [24, 25]. This allows for MnO to open the so-called optical bandgap (lowest direct dipole-allowed transition energy) of about 2 eV [26]. The fundamental bandgap and the spin magnetic moment are equal to 3.9 eV [27] and 4.58–4.79 $\mu_B$ [23, 28], respectively. The DFT + $U$ approach indicates that the MnO system is a charge transfer/Mott–Hubbard insulator [3, 6].

This paper is aimed at a study of the vibrational properties of the MnO lattice. Analysis is limited to the harmonic approximation. An influence of the Hubbard potential on lattice dynamics and the phonon-dependent thermodynamical functions is discussed. Results of the calculations are compared to the available experimental data.

 

## 2. Methodology

Calculations were performed using the plane-wave basis VASP code [29, 30] which implements the spin-polarized DFT and a projector augmented wave (PAW) technique [31]. The valence electrons of Mn and O were described by the pseudopotential configurations ($3d^6 4s^1$) and ($2s^2 2p^4$), respectively. Exchange and correlations were treated within the generalized gradient approximation (GGA). A plane-wave expansion up to 520 eV was used. Effects of electron correlation beyond GGA were taken into account within the framework of GGA + $U$ and the simplified (rotationally invariant) approach of Dudarev *et al* [25]. For Mn 3d electrons the Coulomb repulsion $U$ was varied from 1 to 7.9 eV, while $J = 1$ eV was kept constant. It should be noted that $U = 6.9$ eV and $J = 0.86$ eV were obtained from constrained DFT calculations by Anisimov *et al* [1].

The Brillouin zone was sampled using the $2 \times 2 \times 2$ $k$-point mesh generated by the Monkhorst–Pack scheme. A combination of conjugate gradient energy minimization and a quasi-Newton force minimization was used to optimize a geometry and the atomic positions of the 64-atom supercell. The atomic positions were relaxed until the forces were smaller than $10^{-5}$ eV Å$^{-1}$. The total energy was converged down to $10^{-7}$ eV.

The phonon dispersion relations and the vibrational density of states (DOS) have been calculated within the harmonic approximation and by using the direct method [32, 33] based on the forces calculated via Hellmann–Feynman theorem. The non-vanishing Hellmann–Feynman (HF) forces, $F_i(n, \mu)$, acting on the atoms $(n, \mu)$ in the supercell, are generated when a single atom $(m, \nu)$ is displaced from its equilibrium position. The following relation between the displacements $u_j(m, \nu)$ and the forces $F_i(n, \mu)$ applies:

$$F_i(n, \mu) = -\sum_j \Phi_{ij}(n, \mu, m, \nu)\, u_j(m, \nu), \tag{1}$$

where $\Phi_{ij}(n, \mu, m, \nu)$ are the force constants. Taking into account the crystal symmetry, $\Phi_{ij}(n, \mu, m, \nu)$ are fitted to the HF forces by a singular value decomposition algorithm. Those force constants are used to construct the dynamical matrix of the system, $\mathbf{D}(\mathbf{k})$, which depends on the wavevector $\mathbf{k}$. Diagonalization of $\mathbf{D}(\mathbf{k})$:

$$\omega^2(\mathbf{k}, j)\, \mathbf{e}(\mathbf{k}, j) = \mathbf{D}(\mathbf{k})\, \mathbf{e}(\mathbf{k}, j), \tag{2}$$

leads to the eigenvalues $\omega(\mathbf{k}, j)$ and the eigenvectors $\mathbf{e}(\mathbf{k}, j)$, which represent the frequencies and polarization vectors of phonons, respectively. Here, the mode index $j$ distinguishes between the phonon branches at the given wavevector $\mathbf{k}$.

For ionic and covalent crystals, the splitting between transverse optic (TO) and longitudinal optic (LO) modes due to the coupling between atomic displacements and a long-range macroscopic electric field is calculated via the non-analytical term added to the dynamical matrix [34]. The non-analytical contributions takes on the following form [32, 35, 36]:

$$\frac{4\pi e^2}{V\epsilon_\infty \sqrt{M_\mu M_\nu}} \times \frac{[\mathbf{k}\cdot\mathbf{Z}^*(\mu)]_\alpha [\mathbf{k}\cdot\mathbf{Z}^*(\nu)]_\beta}{|\mathbf{k}|^2} \times \exp\{-2\pi i \mathbf{g}\cdot[\mathbf{r}(\mu) - \mathbf{r}(\nu)]\} \frac{1 + \cos(\pi|\mathbf{k}|/|\mathbf{k}_{BZ}|)}{2}, \tag{3}$$

where $\mathbf{k}$ is the wavevector within a Brillouin zone with a center at the reciprocal lattice vector $\mathbf{g}$ and $\mathbf{k}_{BZ}$ stays for the wavevector parallel to $\mathbf{k}$ having the length from the Brillouin zone center to the Brillouin zone surface. Symbols $V$, $M_\mu$ and $\mathbf{r}_\mu$ denote the volume of the primitive unit cell, atomic masses and positions, respectively. The Born effective charge tensors and the high-frequency dielectric constant are denoted by $\mathbf{Z}^*(\mu)$ and $\epsilon_\infty$, respectively.

The partial phonon density of states describes the contribution to the density of states for the selected atom $\mu$ vibrating along a selected Cartesian coordinate $i$. It is defined as [32]

$$g_{i,\mu}(\omega) = \frac{1}{nd\Delta\omega} \sum_{\mathbf{k},j} |e_i(\mathbf{k}, j; \mu)|^2 \delta_{\Delta\omega}(\omega - \omega(\mathbf{k}, j)), \tag{4}$$

where $e_i(\mathbf{k}, j; \mu)$ is the $i$th Cartesian component of the eigenvector of the mode $(\mathbf{k}, j)$ for the atom $\mu$, $\Delta\omega$ denotes the frequency interval, $n$ is the number of sampling wavevector points, $d$ stands for the dimension of $\mathbf{D}(\mathbf{k})$, while $\delta_{\Delta\omega}(x)$ equals 1 if $|x| \leqslant \Delta/2$, otherwise it is equal to zero. The total vibrational density of states can be obtained from the following relation:

$$g(\omega) = \sum_{i,\mu} g_{i,\mu}(\omega). \tag{5}$$

In the harmonic approximation $g(\omega)$ is used to evaluate the lattice contribution to the heat capacity which is expressed as follows:

$$C = Nrk_B \int_0^\infty d\omega\, g(\omega) \left(\frac{\hbar\omega}{k_B T}\right) \frac{\exp(\frac{\hbar\omega}{k_B T})}{[\exp(\frac{\hbar\omega}{k_B T}) - 1]^2}, \tag{6}$$

where $N$ is the number of primitive unit cells, $r$ stands for the number of degrees of freedom in the unit cell, $T$ is the temperature, and $k_B$ and $\hbar$ denote the Boltzmann and Planck constants, respectively.

The phonon density of states enables us to calculate a thermal motion of atoms which enter the form factor describing an intensity of the radiation scattered by the crystal. Such a form factor contains the Debye–Waller factor defined as $\exp\{-W_\mu(\mathbf{k})\}$, where

$$W_\mu(\mathbf{k}) = \tfrac{1}{2}(2\pi\mathbf{k}\cdot\mathbf{B}(\mu)\cdot(2\pi\mathbf{k})). \tag{7}$$

The $\mathbf{B}(\mu)$ represents the static correlation function of the $\mu$ th atom displacements, $U(\mu)$, from its equilibrium position and it is a second-rank symmetric tensor having the following components:

$$B_{ij}(\mu) = \langle U_i(\mu) U_j(\mu)\rangle. \tag{8}$$

The tensor $\mathbf{B}(\mu)$ represents the mean-squared displacement of the atom $\mu$ and it is expressed by the diagonal and off-diagonal partial phonon density of states $g_{il,\mu}(\omega)$ taking on the following form [32]:

$$B_{il}(\mu) = \frac{\hbar r}{2M_\mu} \int_0^\infty d\omega\, g_{il,\mu}(\omega)\, \omega^{-1} \coth\left(\frac{\hbar\omega}{2k_B T}\right), \tag{9}$$

where the symbol $M_\mu$ denotes the mass of the atom $\mu$.

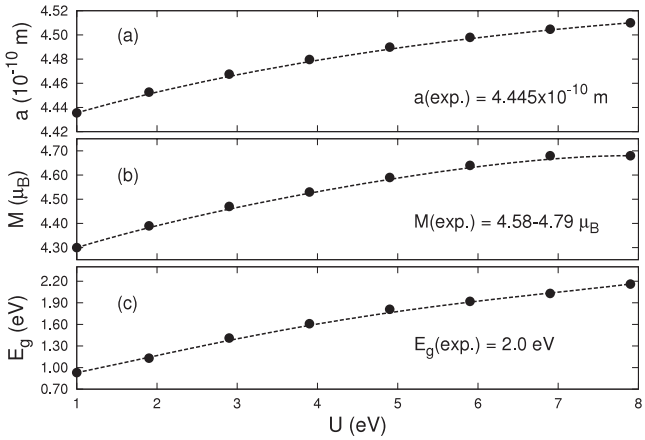


**Figure 1.** Variation of lattice constant ($a$), magnetic moment ($M$) and energy gap ($E_g$) with $U$ for MnO. The exchange parameter $J$ is kept constant at 1 eV. Experimental values of $a$, $M$ and $E_g$ are taken from [19], [23, 28], and [27], respectively.

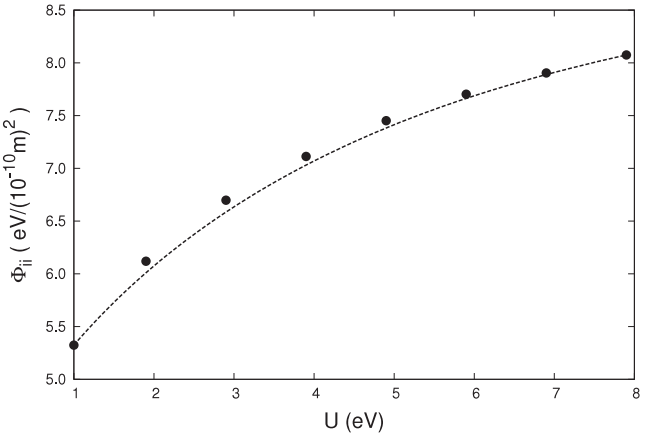


**Figure 2.** Variation of the on-site force constant on Mn ($\Phi_{ii}$) upon the applied $U$.

In the present calculations, a small trigonal distortion from the rocksalt structure is neglected and therefore one considers only two crystallographically non-equivalent atoms, i.e. Mn and O. The HF forces are generated by displacing Mn and O atoms from their equilibrium position by 0.03 Å. Both positive and negative displacements are applied to minimize the systematic errors. Hence, four displacements are calculated.

For a nearly cubic symmetry of MnO, the tensors of Born effective charges reduce to a diagonal tensor with a single element $Z^*_{\mathrm{Mn}} = -Z^*_{\mathrm{O}} = |Z^*|$. The Born effective charges, $|Z^*| = 2.2$, for Mn and O have been estimated using the $q \to 0$ limit technique and the Lyddane–Sachs–Teller relation ($\omega^2_{\mathrm{LO}} - \omega^2_{\mathrm{TO}} \sim |Z^*|^2/\epsilon_\infty$). The transverse optic frequency $\omega_{\mathrm{TO}} = 7.86$ THz and longitudinal optic frequency $\omega_{\mathrm{LO}} = 14.51$ THz have been taken from experiments performed by Haywood *et al* [10], while $\epsilon_\infty = 4.95$ has been adopted from [37, 38]. It should be mentioned that a similar value of $|Z^*|$ has been used in other theoretical studies of lattice dynamics of MnO [5, 6].

## 3. Results and discussion

The influence of $U$ on the structural, magnetic and electronic properties of MnO is shown in figure 1. The lattice constant increases by about 2% with increasing $U$, while the magnetic moment changes by 9%. The best agreement between the experimental and calculated lattice constants is found for the lowest values of $U$. The experimental magnetic moment is reached for $U > 5$ eV. Of course, the most sensitive to the choice of $U$ is the energy gap. The calculated bandgap of 2.0 eV is encountered for $U > 6$ eV and it stays in agreement with the calculated optical bandgap, the latter obtained for $U = 6.9$ eV by the full-potential linearized augmented plane-wave method [3]. For $U > 6$ eV we approach the experimental value of the optical bandgap (2.0 eV [26]), while the experimental value of 3.9 eV determined by van Elp *et al* [27] is unlikely to be obtained even for very high $U$. This apparent disagreement has been discussed by Tran *et al* [3].

Calculations of the lattice vibrations have been performed for $U$ ranging from 1 to 7.9 eV. Therefore, one could obtain a variation of the force constants upon the applied $U$ as shown in figure 2. The on-site force constant on Mn increases from 5.32 to 8.08 eV Å$^{-2}$ while increasing $U$ from 1 to 7.9 eV. Such a pronounced increase in the force constants (50%) cannot be assigned to a modification of the crystal geometry since we observe only a small increase in Mn–O distances. When $U$ changes from 1 to 7.9 eV, the bond length changes from 2.22 to 2.25 Å. Therefore, an enhancement in the force constants can be assigned to the charge redistribution due to the increased Coulomb repulsion on Mn. The higher $U$ localizes more strongly the 3d electrons of Mn and prevents the charge flow. The force constants on oxygen are not so strongly affected by $U$. The Hubbard $U$ approaching 7.9 eV increases the force constant at the oxygen site by about 29% as compared to the force constant calculated with $U = 1$ eV. Hence, the oxygen force constants experience the changes indirectly.

The force constants modified by the term $U$ affect those crystal properties which are phonon-dependent. One can expect to obtain a quite significant change in the calculated phonon dispersion relations and in the phonon density of states (DOS). The calculated phonon dispersion curves with $U = 1$ and 7.9 eV are shown in figures 3 and 4, respectively. They are compared to the inelastic neutron scattering data measured at room temperature by Haywood *et al* [9, 10]. Calculations are also compared to the recent inelastic neutron scattering data obtained at low temperature (4.3 K) by Chung *et al* [13]. It should be noted that in the latter experiment only the transverse optical phonon modes have been measured. When $U = 1$ eV is applied, the calculated phonon branches remain significantly underestimated as compared to the experimental data. Frequencies of both transverse and longitudinal modes belonging to either acoustic or optical phonons are too small. Only the longitudinal acoustic modes (LA) along the [$\xi\xi\xi$] direction seem to be better predicted. One has to note that this branch also reproduces the experimental data with a reasonable accuracy at $U = 7.9$ eV.

In the whole Brillouin zone of MnO, the transverse optical (TO) and longitudinal optical (LO) phonons move upward with

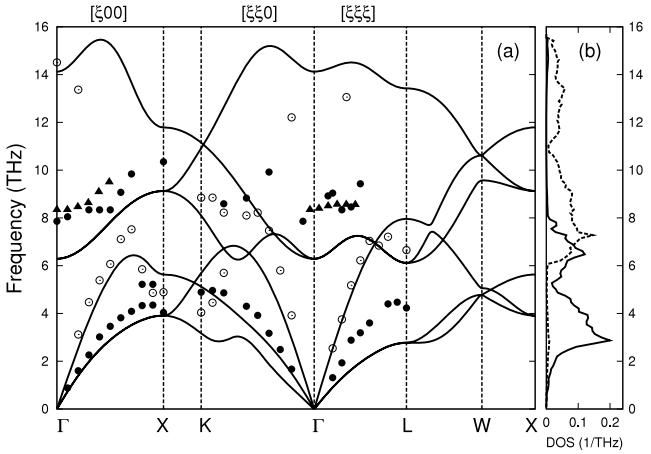


**Figure 3.** (a) Phonon dispersion relations of MnO calculated with $U = 1$ eV (solid line). Inelastic neutron scattering data measured at room temperature [9, 10] are shown by solid and open circles. Solid triangles denote inelastic neutron scattering data obtained at 4.3 K [13]. Transverse and longitudinal modes are indicated by solid and open symbols, respectively. (b) Partial phonon densities of states of Mn (solid line) and O (dashed line) calculated according to equation (4).

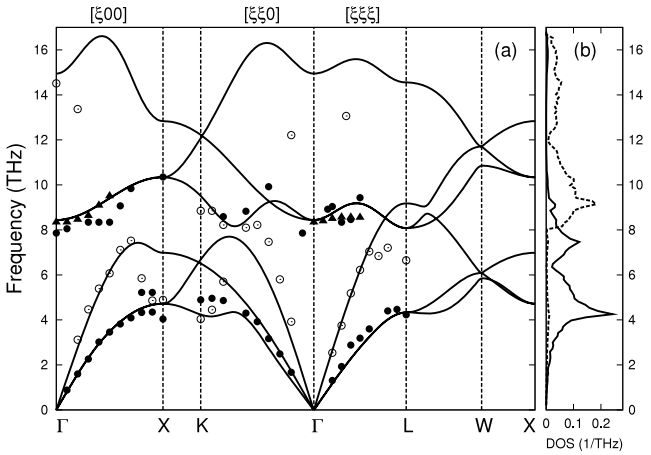


**Figure 4.** (a) Phonon dispersion relations of MnO calculated with $U = 7.9$ eV. Experimental data from inelastic neutron scattering [9, 10, 13] are shown for comparison. (b) Partial phonon densities of states for Mn and O. The same notation as in figure 3 applies.

the increasing $U$. The evolution of TO and LO frequencies at the Γ-point is shown versus $U$ in figure 5. The increase of the zone center TO and LO frequencies amounts to 34% and 6%, respectively. One has to note that the TO frequency is directly calculated from the Hellmann–Feynman forces, while the LO frequency results from the non-analytical term being dependent upon the Born effective charges, the electronic part of the dielectric constant, atomic masses and the volume of the primitive unit cell (see expression (3)). Since the lattice constant of the crystallographic unit cell depends slightly upon $U$ (see figure 1(a)), hence the volume of the primitive cell stays dependent on $U$ as well. When the remaining quantities are kept constant, the volume change amounts to approx. 6%, giving the mentioned increase of the LO frequency. A small

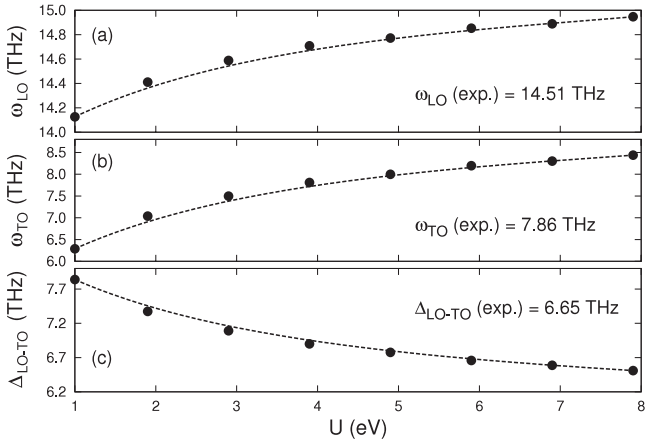


**Figure 5.** (a) Evolution of Γ-point longitudinal optic frequency ($\omega_{LO}$) versus $U$. (b) Evolution of Γ-point transverse optic frequency ($\omega_{TO}$) versus $U$. (c) Evolution of Γ-point LO–TO splitting ($\Delta_{LO-TO}$) versus $U$. Experimental values of the respective frequencies are taken from [9, 10].

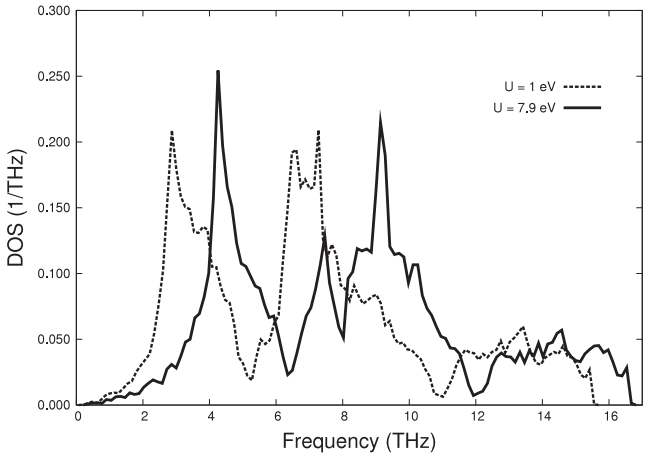


**Figure 6.** Total phonon density of states for MnO calculated with $U = 1$ eV (dashed curve) and $U = 7.9$ eV (solid curve).

variation of $\omega_{LO}$ as compared to a quite significant change of $\omega_{TO}$ results in a decrease of LO–TO splitting as shown in figure 5(c). It should be mentioned that neither low nor high $U$ reproduce the experimental frequencies of LO modes. Only the TO modes in the [ξ00] direction meet the room temperature experimental data [10] for $U = 4.9$ eV (figure not shown). In the [ξ00] direction, the TO branch calculated with $U > 5.9$ eV shows better agreement with the low temperature data [13], while in the [ξξξ] direction it remains slightly overestimated. The zone center $\omega_{TO} = 8.4$ THz and $\omega_{LO} = 14.9$ THz calculated with $U = 7.9$ eV are comparable to the zone center TO and LO frequencies obtained by Savrasov *et al* [5] ($\omega_{TO} = 8.9$ THz, $\omega_{LO} = 15.3$ THz). The calculated $\omega_{TO}$ stays in very good agreement with $\omega_{TO}$ measured at 4.3 K by Chung *et al* [13].

Figure 6 shows the total phonon density of states calculated with $U = 1$ and 7.9 eV. A shift of the phonon spectrum to higher frequencies with the increasing $U$ is observed. This shift is more pronounced for $U$ ranging

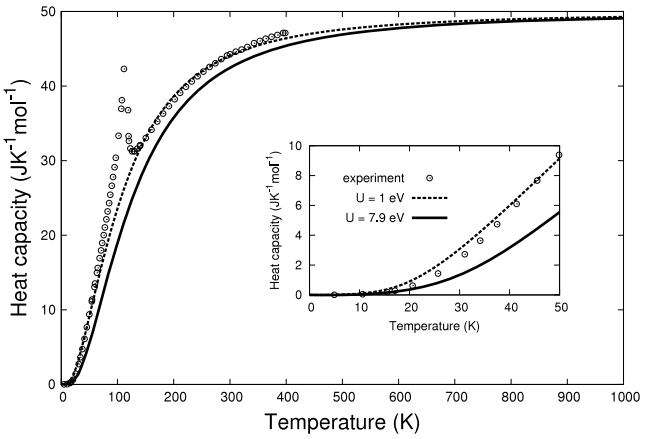


**Figure 7.** Lattice contribution to the heat capacity of MnO calculated with $U = 1$ eV (dashed line) and $U = 7.9$ eV (solid line). Experimental data (open symbols) are taken from [40]. The inset shows respective heat capacities for temperatures lower than 50 K.

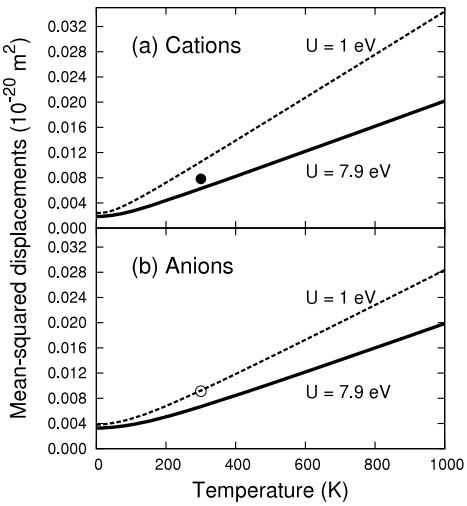


**Figure 8.** Mean-squared displacements versus temperature for cations and anions in MnO crystal calculated using equation (9). Dashed and solid curves represent calculations performed with $U = 1$ and 7.9 eV, respectively. Solid and open symbols denote the experimental thermal vibrations of Mn and O, respectively. Experimental data are taken from [41].

from 1 to 4.9 eV, while the differences between particular phonon densities of states calculated for higher Hubbard terms are rather small. Therefore, the phonon-dependent thermodynamical functions do not exhibit meaningful changes, provided $U > 4.9$ eV is used.

An example is the lattice contribution to the heat capacity, which is calculated from the known phonon density of states using equation (6). One has to note that in the case of MnO the experimental heat capacity contains also the hyperfine and magnon components. The hyperfine contribution is negligible above 10 K, while the magnetic component is relevant between 10 and 150 K [39, 40]. MnO undergoes a magnetic transition at 118 K and hence the experimental heat capacity [40] shows a λ-type behavior in the vicinity of the Néel temperature. The lattice heat capacities calculated for $U = 1$ and 7.9 eV are shown in figure 7. They follow the Debye model and approach the Dulong–Petit limit at high temperatures. A maximal difference between heat capacities calculated with $U = 1$ and 7.9 eV is found at about 100 K and it reaches 0.56 J mol$^{-1}$ K$^{-1}$. This difference becomes negligible at high temperatures, i.e. when the Dulong–Petit law is obeyed. The inset in figure 7 indicates that below 50 K the experimental heat capacity lies inside the range limited by the theoretical lattice heat capacities calculated with low and high $U$. On the other hand, one has to remember that below the Néel temperature the experimental heat capacity of MnO is dominated by the magnetic contribution. Therefore, a simple comparison made between theoretical lattice contributions obtained at different values of $U$ and the total heat capacity cannot indicate unambiguously the value of $U$ reproducing the experimental data. One may suggest that the lattice heat capacity could be better predicted with $U > 5$ eV since for larger $U$ the calculated dispersion curves are closer to those obtained experimentally (see figure 4).

Figure 8 shows the mean-squared amplitude of atomic vibrations (MSD) calculated versus temperature for Mn and O. A comparison between the thermal motions obtained with the lowest and the highest $U$ is made. Theoretical MSD are also compared to the available experimental MSD measured at room temperature [41]. In the entire temperature range, cations have lower MSD than anions due to the difference in their masses. The mean-squared displacements of Mn increase with the decreasing $U$ due to the decreased effective force constant at the Mn site. At very low temperatures the difference between mean-squared displacements of Mn calculated with $U = 1$ and 7.9 eV reaches 30%, while at elevated temperatures it is over two times greater. A similar effect is encountered for oxygens, however they are not so sensitive to the choice of $U$ as cations. At low temperatures the oxygen vibrational amplitude decreases by 17% when $U$ is raised up to 7.9 eV. An agreement between theoretical and the experimental mean-squared displacements measured at room temperature is found for the lower values of $U$. The Hubbard terms of 1 and 3 eV give the experimental MSD for O and Mn, respectively.

The averaged MSD slope can be used to estimate the Debye temperature ($\Theta_D$) of MnO. The MSD slopes decrease with the increasing $U$ and hence this results in the increase of $\Theta_D$ while elevating $U$. The Debye temperature of MnO calculated for $U = 1$ and 7.9 eV amounts to 347 and 439 K, respectively. Both values remain underestimated as compared to $\Theta_D = 515$ K estimated from the low temperature heat capacity measurements [40].

## 4. Summary and conclusions

The on-site Coulomb interactions between 3d electrons, represented by the Hubbard energy $U$, are crucial for the description of the lattice dynamics of MnO. Calculations carried out with too low repulsion in 3d electron shell result in the underestimation of the phonon dispersion curves due to the underestimated Hellman–Feynman forces. The room temperature frequencies of the phonon dispersion relations

are reproduced with a reasonable accuracy using $U$ of about 5 eV. The higher Hubbard energies are required to obtain better agreement with the low temperature transverse optic phonons. The calculated phonon density of states is affected by $U$ as well. The higher Coulomb interactions shift the phonon spectrum to higher frequencies. Therefore, thermodynamical functions which depend on the phonon density of states also experience changes. The differences between results obtained for $U < 5$ eV are quite significant and they become negligible when higher $U$ are applied.

## Acknowledgment

The Interdisciplinary Modeling Center (ICM), Warsaw University, Poland, is acknowledged for providing the computer facilities under grant no. G28-12.

## References

[1] Anisimov V I, Zaanen J and Andersen O K 1991 *Phys. Rev.* B **44** 943
[2] Anisimov V I, Solovyev I V, Korotin M A, Czyzyk M T and Sawatzky G A 1993 *Phys. Rev.* B **48** 16929
[3] Tran F, Blaha P, Schwarz K and Novák P 2006 *Phys. Rev.* B **74** 155108
[4] Dudarev S L, Peng L M, Savrasov S Y and Zuo J M 2000 *Phys. Rev.* B **61** 2506
[5] Savrasov S Y and Kotliar G 2003 *Phys. Rev. Lett.* **90** 056401
[6] Massidda S, Posternak M, Baldereschi A and Resta R 1999 *Phys. Rev. Lett.* **82** 430
[7] Wdowik U D and Parlinski K 2007 *Phys. Rev.* B **75** 104306
[8] Sakurai J, Buyers W J L, Cowley R A and Dolling G 1968 *Phys. Rev.* **167** 510
[9] Haywood B C G and Collins M F 1969 *J. Phys. C: Solid State Phys.* **2** 46
[10] Haywood B C G and Collins M F 1971 *J. Phys. C: Solid State Phys.* **4** 1299
[11] Reichardt W, Wagner V and Kress W 1975 *J. Phys. C: Solid State Phys.* **8** 3955
[12] Coy R A, Tompson C W and Gürmen E 1976 *Solid State Commun.* **18** 845
[13] Chung E M L, Paul D McK, Balakrishnan G, Lees M R, Ivanov A and Yethiraj M 2003 *Phys. Rev.* B **68** 140406(R)
[14] Upadhyaya K S and Singh R K 1974 *J. Phys. Chem. Solids* **35** 1175
[15] Gupta B R K and Verma M P 1977 *J. Phys. Chem. Solids* **38** 929
[16] Agarwal S K 1979 *Solid State Commun.* **29** 197
[17] Upadhyaya K S, Upadhyaya G K and Pandey A N 2002 *J. Phys. Chem. Solids* **63** 127
[18] Luo W, Zhang P and Cohen M L 2007 *Solid State Commun.* **142** 504
[19] Jeanloz R and Rudy A 1987 *J. Geophys. Res.* **92** 11433
[20] Boire R and Collins M F 1977 *Can. J. Phys.* **55** 668
[21] Bloch D, Vettier C and Burlet P 1980 *Phys. Rev. Lett.* A **75** 301
[22] Roth W L 1958 *Phys. Rev.* **110** 1333
[23] Cheetham A K and Hope D A O 1983 *Phys. Rev.* B **27** 6964
[24] Liechtenstein A I, Anisimov V I and Zaanem J 1995 *Phys. Rev.* B **52** R5467
[25] Dudarev S L, Botton G A, Savrasov S Y, Humphreys C J and Sutton A P 1998 *Phys. Rev.* B **57** 1505
[26] Huffman D, Wild R L and Shinmei M 1969 *J. Chem. Phys.* **50** 4092
[27] van Elp J, Potze R H, Eskes H, Berger R and Savatzky G A 1991 *Phys. Rev.* B **44** 1530
[28] Fender B E F, Jacobson A J and Wedgwood F A 1968 *J. Chem. Phys.* **48** 990
[29] Kresse G and Furthmüller J 1999 *Computer code VASP* Vienna, Austria
[30] Kresse G and Furthmüller J 1996 *Phys. Rev.* B **54** 11169
[31] Kresse G and Joubert J 1999 *Phys. Rev.* B **59** 1758
[32] Parlinski K 2008 *Software PHONON* Cracow, Poland
[33] Parlinski K, Li Z-Q and Kawazoe Y 1997 *Phys. Rev. Lett.* **78** 4063
[34] Pick R M, Cohen M H and Martin R M 1970 *Phys. Rev.* B **1** 910
[35] Parlinski K and Kawazoe Y 1999 *Phys. Rev.* **60** 15511
[36] Parlinski K, Li Z-Q and Kawazoe Y 2000 *Phys. Rev.* **61** 272
[37] Gielisse P J, Plendl J N, Mansur L C, Marshall R, Mitra S S, Mikolajewicz R and Smakula A 1965 *J. Appl. Phys.* **36** 2446
[38] Plendl J N, Mansur L C, Mitra S S and Chang I F 1969 *Solid State Commun.* **7** 109
[39] Woodfield B F, Wilson M L and Byers J M 1997 *Phys. Rev. Lett.* **78** 3201
[40] Shapiro J L, Woodfield B F, Stevens R, Boerio-Goates J and Wilson M L 1999 *J. Chem. Thermodyn.* **31** 725
[41] Sasaki S, Fujino K, Takeuchi Y and Sadanaga R 1980 *Acta Crystallogr.* A **36** 904